

## Role of the effective mass and interfacial dipoles on exciton dissociation in organic donor-acceptor solar cells

Christian Schwarz,<sup>1</sup> Steffen Tscheuschner,<sup>1</sup> Johannes Frisch,<sup>2</sup> Stefanie Winkler,<sup>2,3</sup> Norbert Koch,<sup>2,3</sup> Heinz Bässler,<sup>1</sup> and Anna Köhler<sup>1,\*</sup>

<sup>1</sup>*Experimental Physics II and Bayreuth Institute of Macromolecular Research (BIMF), University of Bayreuth, 95440 Bayreuth, Germany*

<sup>2</sup>*Institut für Physik, Humboldt-Universität zu Berlin, 12489 Berlin, Germany*

<sup>3</sup>*Helmholtz-Zentrum Berlin für Materialien und Energie GmbH, 12489 Berlin, Germany*

(Received 25 February 2013; published 15 April 2013)

Efficient exciton dissociation at a donor-acceptor interface is the crucial, yet not fully understood, step for obtaining high efficiency organic solar cells. Recent theoretical work suggested an influence of polymer conjugation length and of interfacial dipoles on the exciton dissociation yield. This necessitates experimental verification. To this end, we measured the dissociation yield of several polymer/C<sub>60</sub> planar heterojunction solar cells up to high electric fields. The results indeed prove that the yield of exciton dissociation depends strongly on the conjugation length of the polymers. Complementary photoemission experiments were carried out to assess the importance of dipoles at the donor-acceptor interfaces. Comparison of exciton dissociation models with experimental data shows that the widely used Onsager-Braun approach is unsuitable to explain photodissociation in polymer/C<sub>60</sub> cells. Better agreement can be obtained using “effective mass” models that incorporate conjugation length effects by considering a reduced effective mass of the hole on the polymer and that include dielectric screening effects by interfacial dipoles. However, successful modeling of the photocurrent field dependence over a broad field range, in particular for less efficient solar cell compounds, requires that the dissociation at localized acceptor sites is also taken into account.

DOI: [10.1103/PhysRevB.87.155205](https://doi.org/10.1103/PhysRevB.87.155205)

PACS number(s): 72.20.Jv, 88.40.jr, 72.80.Le

### I. INTRODUCTION

Organic solar cells have now reached power conversion efficiencies above 10%, which is often referred to as the lower limit for industrial mass production.<sup>1</sup> A significant contribution to this advance lies in the optimization of film-processing conditions and device architecture.<sup>2–6</sup> These steps serve to increase the fraction of photogenerated excitons that can dissociate, e.g., by reaching dissociation sites, and effectively reduce inadvertent recombination of electrons and holes.<sup>7</sup> For even more efficient solar cells, fill factor, short circuit current, and open circuit voltage need to be improved by increasing the exciton dissociation yield further.<sup>8</sup> A key step toward this lies in understanding the mechanisms and the material parameters that control how a photogenerated bound electron-hole (e-h) pair (exciton) dissociates into mobile charge carriers. Knowledge of the relevant processes allows for further optimization of film morphology and device architecture and, in particular, for guidelines in the design and choice of suitable high efficiency materials.

Today’s organic solar cells involve at least two different types of molecular materials, i.e., a donor compound and an acceptor. In such a donor-acceptor (D-A) system, an exciton is created next to a molecular D-A interface or reaches it within its lifetime. There, it transfers its electron from the excited donor to the ground state acceptor molecule and forms a charge transfer state. This initial charge transfer step usually takes place on an ultrafast timescale.<sup>9,10</sup> Since the dielectric constant of organic semiconductors is typically only 3–4, dielectric screening is weak and the e-h pair is initially bound by its Coulomb potential. To become mobile, the charges need to escape from their mutual Coulombic potential without suffering geminate recombination. In a naïve picture

of pointlike charges, they are unbound when they separate to a distance defined as the capture radius, which, in the absence of an electrostatic field, is  $r_c = e^2/4\pi\epsilon_0\epsilon_r kT$ . At that distance, the thermal energy exceeds the Coulomb energy, with typical room temperature values being  $r_c \cong 16$  nm for  $\epsilon_r = 3.5$ .

The central question is why the e-h pair can overcome the considerable Coulomb potential. One currently discussed possibility is that the excess energy, liberated when the excited donor electron transfers to the acceptor, facilitates complete dissociation. In this case, the yield should depend on the energy difference between the energy of the lowest unoccupied molecular orbital (LUMO) level of the donor and the acceptor. Although there are reports in the literature in favor of this possibility,<sup>11–13</sup> there is strong evidence that alternative dissociation channels must be operative as well. Experimental and theoretical investigations suggest that the degree of delocalization of both an exciton and a charge in a conjugated polymer may be of key importance,<sup>9,12,14–16</sup> the extreme view being the notion that conjugated polymers behave like a one-dimensional inorganic semiconductor with completely delocalized wavefunctions.<sup>17</sup> A more conservative view is that right after its creation, an e-h pair at a D-A interface is in a short-lived extended state with a high, yet finite chance for complete dissociation. Unsuccessful e-h pairs relax in energy and form more tightly bound meta-stable charge transfer states, from which subsequent dissociation attempts may occur.<sup>12</sup> In addition to exciton delocalization, it has emerged that interfacial dipoles may also be conducive to exciton dissociation. Theoretical,<sup>18,19</sup> as well as experimental,<sup>20</sup> evidence for such dipoles seems to correlate with increased photocurrent yields.

To discriminate between the different possibilities, one may compare the experimental photocurrent yields against

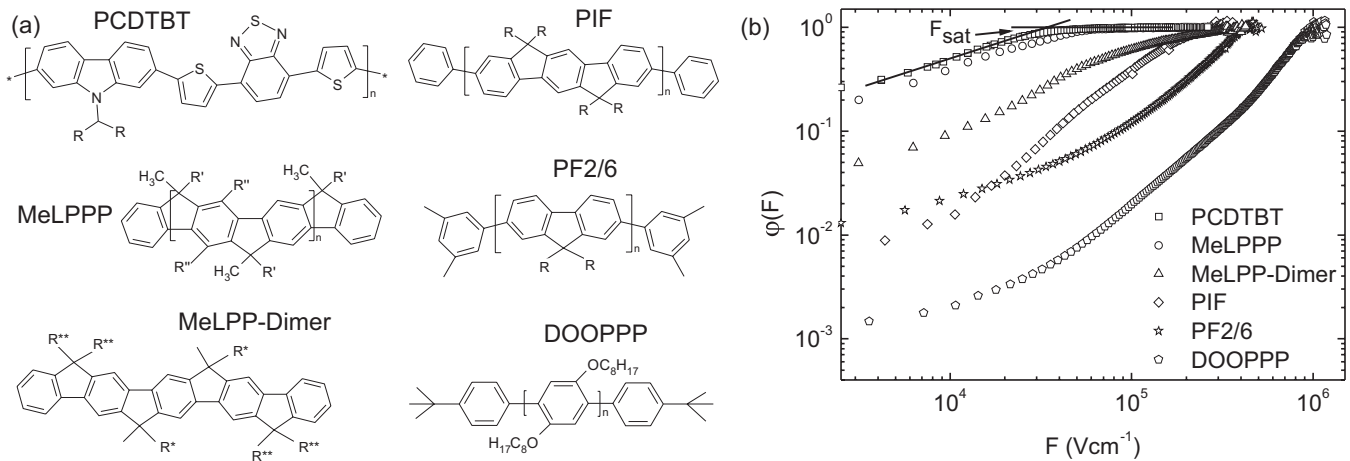


FIG. 1. (a) Chemical structures and abbreviations of the donor polymers ( $R = 2$ -ethylhexyl,  $R' = 1,4$ - $C_6H_4$ - $n$ - $C_{10}H_{21}$ ,  $R'' = -n$ - $C_6H_{13}$ ,  $R^* = C_6H_{13}$ ,  $R^{**} = C_{10}H_{13}$ ). (b) External photocurrent quantum yields of bilayer  $C_{60}$  devices made with PCDTBT, MeLPPP, MeLPPP-dimer, PIF, PF2/6, and DOOPPP, measured at 2.2 eV excitation as a function of the internal field and normalized to unity at the saturation value. For PCDTBT, the tangents whose intersection defines the saturation field  $F_{sat}$  are indicated as an example. PCDTBT = Poly[[9-(1-octyl)nonyl]-9H-carbazole-2,7-diyl]-2,5-thiophenediyl-2,1,3-benzothiadiazole-4,7-diyl-2,5-thiophenediyl], MeLPPP = methyl-ladder-type-poly(*p*-phenylene), MeLPPP-dimer = methyl-ladder-type-*p*-phenylene-dimer, PIF = poly(indeno-fluorene), PF2/6=ethyl-hexyl-poly(fluorene), DOOPPP = Di-octyloxy-poly(*p*-phenylene).

predictive models. A classical approach, based on the seminal works by Onsager and Braun, consists in considering the dependence of exciton dissociation on an increasing electric field in the device.<sup>21</sup> A coulombically bound e-h pair requires a certain electric field for complete separation. Above a certain saturation field strength, the yield should become constant when the drop of the electrostatic potential exceeds the Coulomb-binding energy of the e-h pair. If geminate recombination was the dominant recombination process, then the saturation field strength  $F_{sat}$  is a measure of the Coulomb-binding energy of an e-h pair and also of the size, i.e., the mean e-h separation of the dissociating e-h pair. While the Onsager-Braun model is frequently employed to interpret organic solar cell performance, its premise of treating the e-h pair as point charges renders its application questionable for materials with extended, delocalized excited states such as polymers. Meanwhile, there are more sophisticated models available. For example, the delocalization of the photogenerated charges can be incorporated explicitly by considering their effective mass.<sup>22–25</sup> Similarly, the screening effect of interfacial dipoles on the Coulomb potential of the e-h pair has been implemented in the theoretical framework.<sup>23,25</sup> So far, however, these models have not yet been compared against experimental data.

Here, we aim to assess the impact of conjugation length and interfacial dipoles on exciton dissociation by comparing simulations of the aforementioned models with experimental data. We recently measured the field dependent photocurrent in a bilayer solar cell in which conjugated phenylene-type donor polymers were combined with a  $C_{60}$  acceptor layer. We found that the more ordered, and thus the more conjugated, a polymer chain is, the lower the saturation field strength.<sup>16</sup> To cover a wide range of donor materials in the same series of experiments and under exactly the same experimental conditions, we confirmed the previous experiments on DOOPPP, PIF, and MeLPPP and expanded them to further include PF2/6, a dimer of MeLPPP and the widely used low band-gap material

PCDTBT (see Fig. 1 for chemical structure and abbreviations). To obtain information on possible interfacial dipoles, ultraviolet photoelectron spectroscopy (UPS) experiments were carried out for the interfaces of these compounds with  $C_{60}$ . The experimental results were analyzed by parameterizing and simulating the existing models. We are able to quantify the effect of charge delocalization, expressed in terms of the effective mass, and of ground state dipoles on the field dependent exciton dissociation. Further, we show that a single mechanism cannot explain the field dependence of the photocurrent, yet it can be modeled adequately by considering a superposition of two processes.

## II. EXPERIMENTAL RESULTS

Figure 1 shows the chemical structures of the investigated polymers and the dimer, as well as the relative photocurrent quantum yields  $\varphi(F)$  of bilayer devices (with  $C_{60}$  as acceptor) as a function of the internal electric field. The key parameter derived from these data is the saturation field strength  $F_{sat}$ , defined by the intersection of the tangents to the photocurrent in the regimes of low electric field and high electric field (i.e., at photocurrent saturation) in a double logarithmic plot (see Fig. 1). The existence of the saturation field implies that there is a field-dependent recombination mechanism that can be overcome at high fields. This can be seen by considering that photoexcitation with rate  $G$  results in bound or unbound charge carriers. This leads to a photocurrent that is controlled by the competition between a field-dependent escape rate  $\mu F/d$  from the recombination zone, with  $\mu F$  being the transport velocity and  $d$  the layer thickness, and a recombination rate  $k_r$ . The recombination mechanism may, in principle, be geminate or nongeminate. The photocurrent then depends on the field as  $j \propto G \cdot \mu F d^{-1} / (\mu F d^{-1} + k_r) = G \cdot 1 / (1 + \frac{dk_r}{\mu F})$ . Thus, at low fields, the photocurrent will be reduced due to recombination, while at high field, it eventually saturates. We

now argue that, in our case, this recombination is predominantly geminate. As detailed in the Supplemental Material,<sup>26</sup> one can estimate that monomolecular and bimolecular decay become comparable at a critical light intensity of about  $2 \cdot 10^{18}$  photons/cm<sup>2</sup>s. Our photocells were measured at a photon flux of about  $4 \cdot 10^{15}$  photons/cm<sup>2</sup>s, i.e., at an intensity that is 1/500ths of the intensity where bimolecular recombination becomes important. This is consistent with the observation that for all materials the photocurrents depend linearly on the pump intensity  $I_{\text{ex}}$ . If the carrier would recombine bimolecularly, as were the case for trap-free nongeminate recombination, a dependence such as  $j \propto \sqrt{I_{\text{ex}}}$  should result. The existence of a saturation field at the light intensities used in our experiment therefore shows that there is a field-dependent geminate-pair recombination mechanism. Such a dominant role of geminate recombination is in agreement with reports by other research groups, even when using higher light intensities.<sup>27</sup> When comparing the polymer MeLPPP and the associated dimer MeLPP, one observes a significant drop of  $F_{\text{sat}}$  from  $4 \cdot 10^4$  V cm<sup>-1</sup> to  $2 \cdot 10^5$  V cm<sup>-1</sup>. This is the first clear indication that wave-function delocalization in the donor is important. It turns out that the saturation field strength, and thus the binding energy of the interfacial e-h pair, decreases in the order DOOPPP, PF2/6, PIF, MeLPP-dimer, MeLPPP, and PCDTBT (Fig. 1, and Table II further below). For the poly-*p*-phenylene based systems, yet not for the donor-acceptor copolymer PCDTBT, this also correlates with a red-shift of the absorption [Fig. 2(a)].

The red-shift of the optical spectra within a series of structurally related compounds is a well-established signature of increased delocalization of the  $\pi$ -electron system in conjugated oligomers and polymers. A heuristic way to correlate the transition energy of an oligomer or polymer with a certain number of conjugated monomers is provided in the coupled oscillator model of W. Kuhn.<sup>28,29</sup> In the case of poly-*p*-phenylene-type polymers, the coupling elements are identified with phenylene rings. By using fluorescence spectra of ladder-type phenylene oligomers, one can parameterize the chain-length dependence of the transition energy of a chain of perfectly aligned phenylenes.<sup>30</sup> Deviations from chain

planarity raise the transition energy and can be translated into an effective conjugation length. This parameterization allows extracting the effective conjugation length of the polymers in both absorption and emission. The two values differ as the excited state geometry is usually more planar than the ground state geometry. In addition, in a film of disordered polymers, there is energy transfer from (shorter) absorbing to (longer) emitting chromophores. In Fig. 2(b), we show the saturation field strengths as a function of the effective conjugation length in absorption and fluorescence for the poly-*p*-phenylene-type systems. The dramatic decrease of  $F_{\text{sat}}$  with the increasing conjugation length of the polymers proves that the spatial extent of the conjugation length in a  $\pi$ -conjugated polymer has an important bearing of exciton dissociation in our solar cells. We also note that the MeLPP-dimer, which contains five phenylene units so that  $1/n = 0.2$ , behaves differently. Although  $F_{\text{sat}}$  for the dimer is four times higher than that for the polymer, one expected a much higher value based upon the parameterization data of the conjugation length. This is evident in Fig. 2(b), where  $F_{\text{sat}}$  for the dimer is compared to the saturation field strength for the polymers.

Having established that there is a clear dependence of the saturation field strength on the effective conjugation length, we now consider whether there is an influence of interfacial dipoles that exist at the heterojunction in the ground state. To this end, the energy-level line-up at the polymer/C<sub>60</sub> interfaces was investigated by UPS. C<sub>60</sub> was sequentially deposited by thermal sublimation in ultrahigh vacuum conditions. After each deposition step, valence band and secondary electron cutoff (SECO) spectra were recorded. The typical SECO evolution upon deposition of C<sub>60</sub> on the polymer film is shown for the example of PCDTBT in Fig. 3(a). We observe that the initial work function of the pristine PCDTBT film (4.60 eV) is increased to 4.72 eV upon 8 Å C<sub>60</sub> deposition, and it remains constant for higher C<sub>60</sub> coverage. The valence spectra show the evolution of C<sub>60</sub>-derived molecular levels. The valence band onset of pristine PCDTBT is at a binding energy of 0.63 eV below the Fermi level ( $E_F$ ), as indicated in Fig. 3(a) this yields an ionization energy of 5.23 eV. The position of the PCDTBT valence band onset was found to be independent of the C<sub>60</sub>

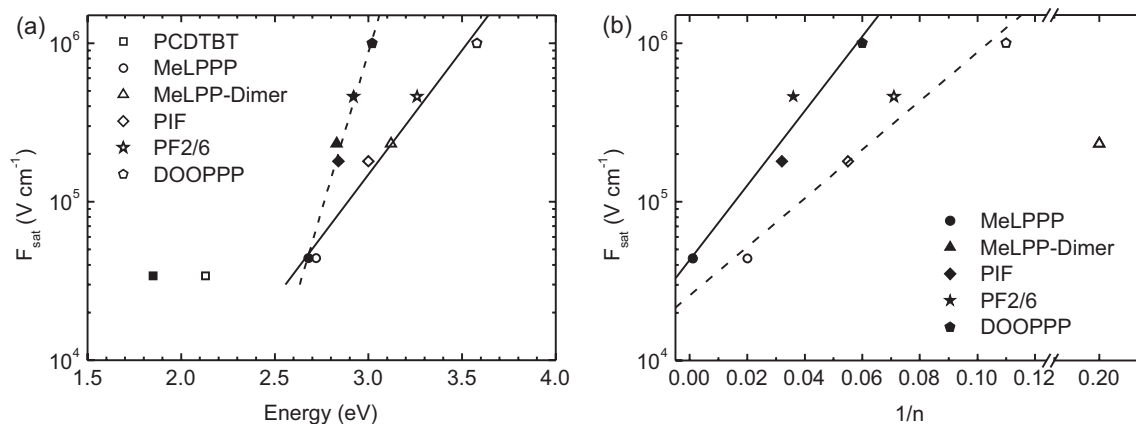


FIG. 2. Saturation field strengths of the bilayer field-dependent photocurrent yields; (a) as a function of the donor absorption energy (empty symbols) and emission energy (filled symbols), (b) as a function of the inverse effective conjugation length of the donors in the ground state geometry (data taken from absorption, empty symbols) and in the excited state geometry (data taken from emission, filled symbols). The lines serve as a guide to the eye.

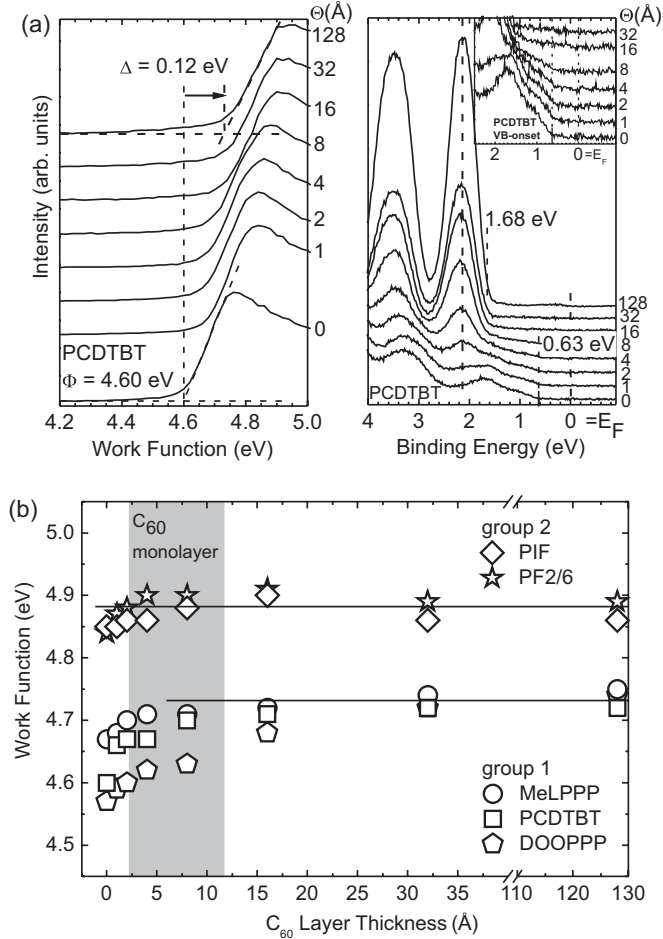


FIG. 3. (a) SECO (left) and low-binding energy region (right) of a 20-nm PCDTBT film spin coated on a PEDOT/PSS-ITO substrate and subsequently deposited  $C_{60}$  on top. (b) Work function evolution as a function of subsequent deposited  $C_{60}$  coverage. Two groups can be distinguished: group 1 (MeLPPP, PCPTBT, and DOOPPP) Fermi-level pinning of  $C_{60}$ -LUMO is found; group 2 (PF2/6 and PIF) vacuum-level alignment is established.

coverage, as it can be observed in the valence band region spectra up to a  $C_{60}$  coverage of 8 Å [see close-up spectra in Fig. 3(b)]. The low binding energy onset of emission from the  $C_{60}$  highest occupied molecular orbital (HOMO) levels is constant at 1.68-eV binding energy for all coverages. Adding the final work function of 4.72 eV to the energy difference between the  $C_{60}$  HOMO onset and the Fermi level yields an ionization energy of 6.40 eV for  $C_{60}$ , which is in line with previously reported values.<sup>31,32</sup>

The situation of a constant HOMO position and an increase of the sample work function for the very early stage of interface formation is typical for an interface dipole due to Fermi-level pinning at unoccupied states of  $C_{60}$ , i.e., the LUMO level or gap states at slightly lower energy.<sup>33,34</sup> In this scenario, the work function changes until a full monolayer is reached and remains constant for higher film thickness, which we indeed observe beyond 8 Å  $C_{60}$  coverage. This coverage corresponds approximately to a monolayer of  $C_{60}$  since the diameter of a  $C_{60}$  molecule is  $\sim 10$  Å.<sup>35</sup> Similar results are obtained for DOOPPP and MeLPPP. In both cases, the initial work function

TABLE I. The ionization energy (IE), the work function  $\Phi$  of the pristine film, and the change in work function  $\Delta\Phi$  due to the deposition of  $C_{60}$ , along with the derived value for the fractional dipole strengths  $\alpha$ .

Material	PCDTBT	MeLPPP	PIF	PF2/6	DOOPPP
IE (eV)	5.23	5.28	5.82	5.85	5.22
$\Phi$ (eV)	4.60	4.67	4.85	4.84	4.57
$\Delta\Phi$ (eV)	0.12	0.08	0.02	0.05	0.17
$\alpha$ ( $10^{-3}$ )	21.4	14.2	3.6	8.9	30.3

of the pristine polymer films increases due to  $C_{60}$  deposition. Note that in all three cases, including PCDTBT, the final work function of a multilayer  $C_{60}$  deposited film onto the polymer film reaches the same value. Thus, ground state interface dipoles of varying magnitude, dependent on the initial polymer work function, are found (Table I). In contrast, vacuum-level alignment was found at the  $C_{60}$ /PIF and  $C_{60}$ /PF2/6 interfaces [Fig. 3(b)]. Within accuracy of our measurement ( $\pm 0.05$  eV), the work function of the PIF and PF2/6 polymers film did not change due to  $C_{60}$  deposition. The evolution of the sample work function as a function of  $C_{60}$  coverage is summarized in Fig. 3(b) for all five different polymers. As indicated in Fig. 3, a transition from vacuum-level alignment to Fermi-level pinning at the polymer/ $C_{60}$  interface occurs for a work function of a pristine polymer film below  $\sim 4.75$  eV. Nevertheless, Fermi-level pinning at unoccupied states of  $C_{60}$  was unexpected because of the  $C_{60}$  threshold electron affinity of 4.50 eV in the solid phase<sup>31</sup> (obtained by inverse photoelectron spectroscopy). This is 0.25 eV lower as the obtained transition work function of  $\sim 4.75$  eV. This difference can be explained by unoccupied gap states that are created within the  $C_{60}$  film due to impurities coming from the spin-coated polymer films or structural defects. The resulting work function values, ionization energies, and work function changes  $\Delta\Phi$  for the five interfaces are summarized in Table I.

From these studies, two key experimental observations emerge.

(i) The electric field strength  $F_{\text{sat}}$ , at which  $\varphi(F)$  saturates decreases by about a factor of 20–30 in the series DOOPPP, PF2/6, PIF, MeLPP-dimer, MeLPPP, and PCDTBT. This correlates with the bathochromic shift of the  $S_1$ - $S_0$  0-0 transition, except for PCDTBT. This is a strong indication that electronic delocalization of the hole residing on the donor is of key importance.

(ii) The photoemission experiments show that there is, indeed, some ground state charge transfer between donor and acceptor, but this effect is relatively weak. In the case of PF2/6, PIF, and MeLPPP, it is barely noticeable. For DOOPPP and PCDTBT, the interfacial potential drop is 170 meV and 120 meV, respectively.

### III. ANALYSIS AND DISCUSSION

#### A. Individual models

One of the most widely applied models to account for exciton dissociation is the Onsager-Braun model, even though it does not account for the effects of effective conjugation length or for interface dipoles.<sup>36,37</sup> The high popularity of

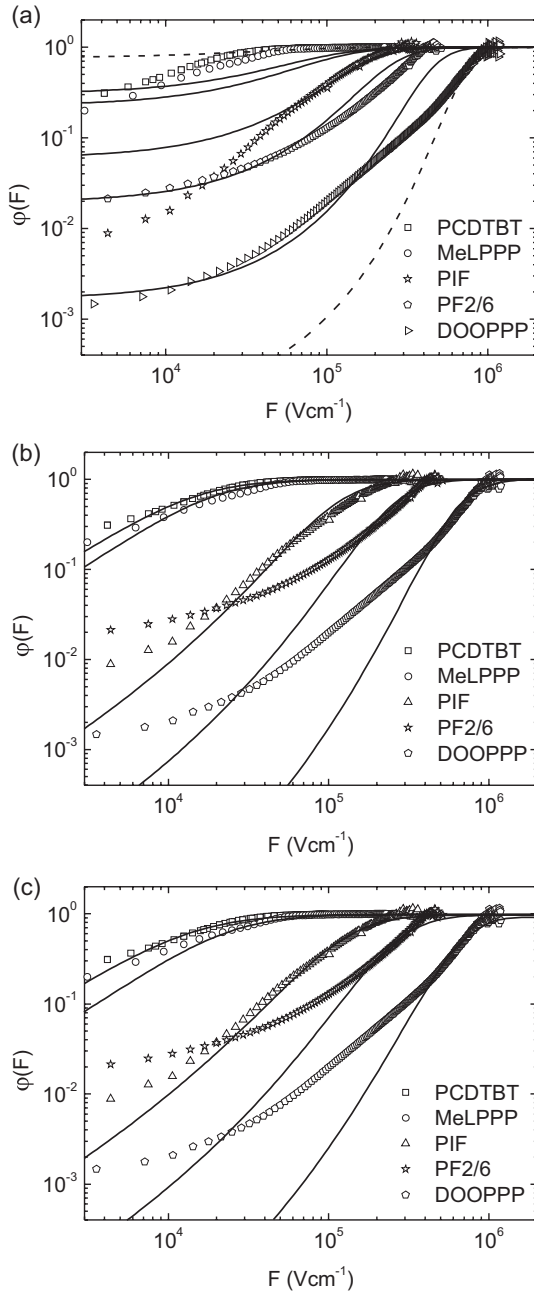


FIG. 4. Comparison of the field-dependent photocurrent yields (symbols) of donor /C<sub>60</sub> bilayer solar cells with simulations (lines) based on (a) the Braun model [Eqs. (1), (2)], (b) the effective mass model [Eqs. (3)–(5)], and (c) the dipole model [Eqs. (3), (6), and (7)]. The parameters are presented in Table II.

this model warrants a detailed consideration. Onsager's theory for photogeneration in a single component molecular solid rests upon the notion that optical excitation with sufficient energy can autoionize and form a Coulombically bound e-h pair.<sup>38</sup> This pair of pointlike charges can rather fully dissociate in the course of temperature and field-assisted random walk of one carrier in the field of the other, or it may recombine geminately to the ground state. Braun extended this concept to D-A systems in which the lowest excited state is a charge transfer state that can live long enough to make several attempts toward complete dissociation before decaying geminately to

the ground state.<sup>39</sup> This dissociation yield is determined by the trade-off between the field-dependent dissociation rate  $k_d(F)$  and the field-independent e-h pair decay rate to the ground state  $k_f$ , i.e.,

$$\varphi(F) = \frac{k_d(F)}{k_d(F) + k_f} = \frac{1}{1 + k_f k_d(F)^{-1}}. \quad (1)$$

The theory predicts a strong field dependence of the dissociation rate  $k_d(F)$ , that is,

$$k_d(F) = \frac{3\mu e}{4\pi\epsilon_0\epsilon_r r_0^3} \exp\left(\frac{-\Delta E}{kT}\right) \frac{J_1(2\sqrt{-2b})}{\sqrt{-2b}} \quad \text{with} \\ b = \frac{e^3 F}{8\pi\epsilon_0\epsilon_r k^2 T^2}. \quad (2)$$

Here,  $J_1$  is the Bessel function of order one,  $F$  is the electric field,  $\mu$  is the sum of the mean electron and hole mobility,  $\Delta E = e^2/4\pi\epsilon_0\epsilon_r r_0$  is the Coulombic-binding energy of the e-h pair, which is controlled by the initial intrapair separation  $r_0$ . Inserting (2) into (1) allows simulating the field dependence of the dissociation yields and comparing it with the experimental data; this is shown in Fig. 4(a). For the simulation, we employed  $\epsilon_r = 3.5$  and we used the Bessel function  $J_1$  and not the frequently employed approximation  $(1 + b + b^2/3 + b^3/18 + \dots)$ , as the deviations become significant in the regime of high field strengths that is of interest here. The free parameters in the simulation are the intrapair separation  $r_0$  and the ratio  $\mu/k_f$ ; they are listed in Table II.

We find that the Onsager-Braun model yields unsatisfactory results in two respects. First, and most importantly, the field dependence for the compounds with low  $F_{\text{sat}}$ , MeLPPP, and PCDTBT, cannot be reproduced at all, and for the remaining compounds, agreement between the experimental data and the Onsager-Braun fits is poor. The main reason for this is that the field dependence predicted by the Braun model is steeper than the experimentally found one. For illustration, if the simulation parameters are adjusted so that there is not an overall agreement with the experimental curve but rather the value of the saturation field is matched [dashed in Fig. 4(a)], one finds that for the regime of low-field strengths, the Onsager-Braun model underestimates the photocurrent yield for DOOPPP while it overestimates it for PCDTBT. Second, the simulation parameters required are unphysical. While the values obtained for  $r_0$  in the nm range are plausible, the values inferred for  $\mu/k_f$  imply either charge mobility or a lifetime that are too high to be consistent with existing knowledge. Consider, for example, PCDTBT, where  $\mu/k_f = 2 \cdot 10^{-8} \text{ cm}^2 \text{ V}^{-1}$ . The lifetime at zero electric field is  $\tau_0 = [k_f + k_d(0)]^{-1}$ .  $k_d(0)$  can be evaluated as  $k_d(0) = \frac{\mu e}{\epsilon_0\epsilon_r} \frac{3}{4\pi r_0^3} \exp(\frac{-\Delta E}{kT})$ . Taking  $\mu$  to be dominated by the hole mobility, and using a value of  $1 \cdot 10^{-4} \text{ cm}^2/\text{Vs}$ ,<sup>40</sup> one obtains  $k_d(0) = 1.3 \cdot 10^3 \text{ s}^{-1}$ ,  $k_f = 5 \cdot 10^3 \text{ s}^{-1}$ , and  $\tau_0 = 158 \mu\text{s}$ . Similar calculations can be carried out for the other polymers in Table II. From this estimate, one can see first that  $k_d(0) < k_f$ , so that  $\tau_0 \approx 1/k_f$ , and, more importantly, the values for  $\tau_0$  range from 6  $\mu\text{s}$  (for MeLPPP, based upon  $\mu = 2 \cdot 10^{-3} \text{ cm}^2/\text{Vs}$ ) to more than 30 ms (for DOOPPP, assuming  $\mu < 10^{-5} \text{ cm}^2/\text{Vs}$ , which is an upper limit for the hole mobility in highly disordered polymers). Typical lifetimes for charge transfer states between

TABLE II. Fit parameter for different individual models, along with the experimentally measured saturation field strength  $F_{\text{sat}}$ .

Material	PCDTBT	MeLPPP	PIF	PF2/6	DOOPPP	MeLPP-dimer
$F_{\text{sat}}$ [Vcm <sup>-1</sup> ]	$3.4 \cdot 10^4$	$4.4 \cdot 10^4$	$1.8 \cdot 10^5$	$4.6 \cdot 10^5$	$1.0 \cdot 10^6$	$2.3 \cdot 10^5$
Onsager-Braun model <sup>a</sup>						
$r_0$ [nm]	1.03	1.02	0.92	0.86	0.80	1.02
$\mu/k_f$ [10 <sup>-12</sup> m <sup>2</sup> V <sup>-1</sup> ]	2.0	1.5	1.3	1.1	0.3	0.50
Effective mass model (numerical)						
$m_{\text{eff}}/m_e$	0.060	0.067	0.110	0.170	0.300	0.115
$\tau_0 \nu_0 \exp(-2\gamma r)$	3910	3830	3500	100	40	3830
Effective mass model (parabolic approximation)						
$m_{\text{eff}}/m_e$	0.060	0.067	0.110	0.170	0.300	0.115
$\tau_0 \nu_0 \exp(-2\gamma r)$	60	65	40	37	12	65
Dipole model						
$m_{\text{eff}}/m_e$	0.117	0.109	0.130	0.250	1.000	0.20
$\tau_0 \nu_0 \exp(-2\gamma r)$	60	65	40	37	12	65

<sup>a</sup>For the solid lines in Fig. 4(a). See Supplemental Material<sup>26</sup> for the dashed lines.

conjugated polymers and C<sub>60</sub> derivatives tend to be up to few tens of nanoseconds.<sup>37,41–43</sup> Thus, the Braun model is clearly inadequate to describe the field dependence of exciton dissociation in conjugated polymers. In the same way, we found the mathematically more rigorous treatment of the Onsager-Braun model presented recently by Wojcik and Tachiya<sup>44</sup> to be inappropriate for these conjugated polymers.

Why should the Onsager-Braun treatment be an unsuitable model for conjugated polymer systems when it has been shown to be highly successful for molecular donor-acceptor crystals? One difference between aromatic molecules such as the polyacenes and the conjugated polymers used in today's solar cells is the degree of charge and exciton delocalization. The experimental results clearly show that the photodissociation yield increases with the effective conjugation length of the polymers. A way to explicitly include the effects due to conjugation has been presented by Arkhipov *et al.* by considering the effective mass of a hole on a polymer chain.<sup>22,23</sup> The original motivation for this effective mass model was the observation of a very weak temperature dependence of the photocurrent in MeLPPP that was incompatible with the predictions of the Onsager-Braun model.<sup>45</sup> Such weak temperature dependence has more recently been confirmed for bilayers<sup>46</sup> as well as blends.<sup>47</sup> In order to account for the lack of temperature activation for a well-conjugated polymer like MeLPPP, Arkhipov suggested there should be an additional term that reduces the energy needed to separation of electron and hole.

The central idea of Arkhipov's model is simple. After photoexcitation of the polymer donor, the electron is transferred to the acceptor, and the hole remains on the polymer chain. The two carriers are bound by their mutual Coulomb potential. The hole on the polymer is delocalized within the effective conjugation length, i.e., it can be viewed to carry out zero-point quantum oscillations in the Coulomb potential due to the electron [Fig. 5(a)]. This quantum oscillation is associated with an energy that depends on the effective mass  $m_{\text{eff}}$  of the hole. This kinetic energy assists the hole in overcoming the Coulomb potential. The effective mass is introduced here in a heuristic way as a measure for the electronic coupling

within the polymer chain that depends on intrachain disorder. A low relative effective mass implies a highly delocalized hole. Arkhipov applied this effective mass model to two different situations. One case comprises the situation of a donor doped with only few acceptors;<sup>22</sup> the other considers an extended interface between donor and acceptor, where dark interfacial dipoles prevail.<sup>23</sup> This idea of the effective mass model has been taken up and developed further by the Baranovskii group. A particularly elegant formulation of the effective mass model has been presented by Nenashev and coworkers, and we have therefore applied the Nenashev formulation to our data.<sup>24</sup> Nenashev considers the polymer as a set of one-dimensional chains that are placed parallel to the polymer fullerene interface. The electric field is acting orthogonal to the interface. The geometry of this model is illustrated in Fig. 5(b). The chains are numbered from 1 to  $n$ , starting at the interface, with spacing  $r$ . The electron on the fullerene is taken as immobile while the hole on the polymer is taken to hop. The dissociation yield  $\varphi(F)$  is controlled by the rates for the recombination of the e-h pair,  $k_r = 1/\tau_0$ , where  $\tau_0$  is the lifetime of the e-h pair, and by the rate for dissociation  $k_d$

$$\begin{aligned} \varphi(F) &= \frac{k_d}{k_d + k_r} = \frac{\tau_0}{\tau_0 + k_d^{-1}} \\ &= \frac{\tau_0}{\tau_0 + \sum_{n=1}^{N-1} a_{n \rightarrow n+1}^{-1} \exp\left(\frac{E_n - E_1}{kT}\right)}. \end{aligned} \quad (3)$$

Here,  $a_{n \rightarrow n+1}$  is the Miller-Abrahams hopping rate of the hole,

$$a_{n \rightarrow n+1} = \nu_0 \exp(-2\gamma r) \begin{cases} \exp\left(-\frac{E_{n+1} - E_n}{kT}\right) & E_{n+1} > E_n \\ 1 & E_{n+1} \leq E_n \end{cases} \quad (4)$$

$\nu_0$  and  $\gamma$  take their usual meaning as frequency factor and as a measure for the electronic coupling, respectively. The hopping and dissociation process is controlled by energy of the hole on each chain,  $E_n$ , which results from the Coulomb potential due to the electron, from the potential of the applied field and from the zero-point oscillation along the conjugated segment within

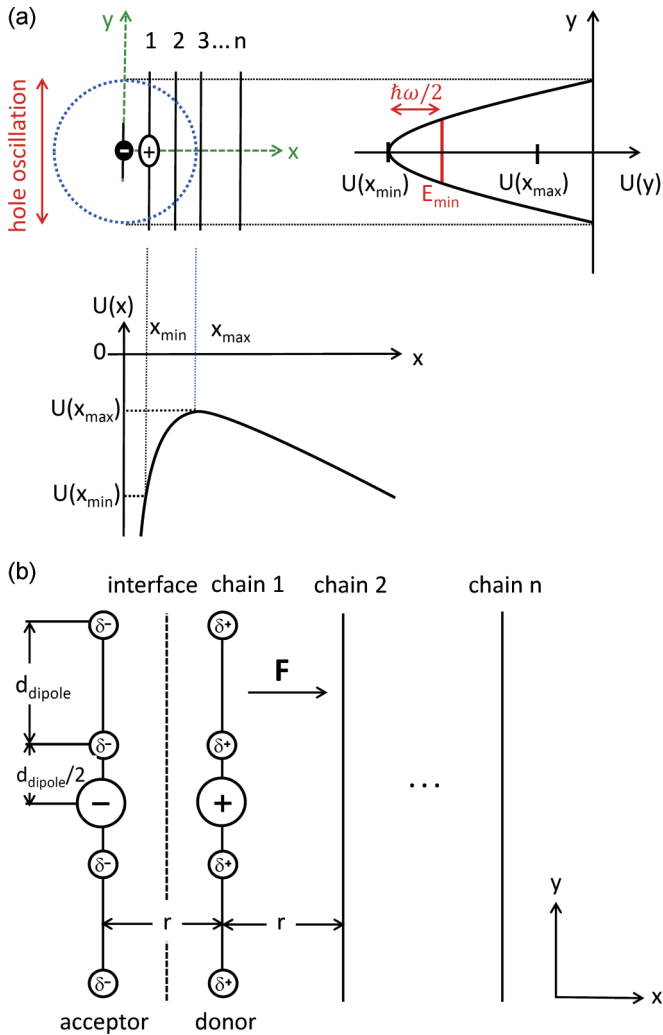


FIG. 5. (Color online) Schematic illustrating electron-hole dissociation at the bilayer interface with an electron on C<sub>60</sub> at  $x = 0$  and a hole on a polymer chain. The chains are assumed parallel to the interface and are labeled 1 to  $n$ . (a) The hole on the polymer chain executes a zero-point oscillation along the  $y$  direction inside the Coulomb well set up by the electron. The potential along  $x$  direction is due to the Coulomb field from an electron at  $x = 0$  and a constant applied electric field in  $x$  direction. The energy of the hole located at  $x_{\min}$  is raised by a zero-point oscillation energy  $\hbar\omega/2$ ,  $E_{\min} = U(x_{\min}) + \hbar\omega/2$ . To escape, the energy barrier between  $E_{\min}$  and  $U(x_{\max})$  needs to be overcome. The potential along the  $y$  direction is approximated by a parabola. (b) Detailed geometry at the donor-acceptor interface. In the effective mass model,  $\delta^+ = \delta^- = 0$ . In the dipole model, interfacial ground state dipoles  $\delta^+$  and  $\delta^-$  modify the potential and assist the hole's escape. For simplicity, we used  $d_{\text{dipole}} = r$  in our modeling.

the Coulomb potential. As detailed in the original paper by Nenashev, it can be calculated solving the Schrödinger equation

$$-\frac{\hbar^2}{2m_{\text{eff}}} \frac{d^2 \psi}{dy^2} + U_n \psi = E_n \psi_n, \quad (5)$$

with

$$U_n = -\frac{e^2}{4\pi\epsilon_0\epsilon_r} \frac{1}{\sqrt{y^2 + x_n^2}} - eFx_n, \quad x_n = nr.$$

The dependence of the dissociation rate on the electric field and on the effective mass is thus included implicitly via the hole energy  $E_n$ . To implement the Nenashev formalism, we solved (5) numerically and inserted the resulting  $E_n$  in (4) and (3), so that  $\varphi(F)$  could be calculated parametric in the relative effective mass  $m_{\text{eff}}/m_e$  and in the product of the e-h pair lifetime with the isoenergetic hopping parameter  $\tau_0\nu_0 \exp(-2\gamma r)$ . The resulting curves with optimized parameters listed in Table II [as “effective mass model (numerical)”) are compared to the experimental data in Fig. 4(b).

In contrast to the Onsager-Braun model, the agreement of the simulated and experimental field dependence is quite satisfactory over the entire field range for the more delocalized compounds PCDTBT, MeLPPP, and PIF. For the compounds with shorter conjugation length, simulation and experiment match only at high fields, and one finds that experimentally there is an additional photocurrent quantum-yield contribution at low field strength. Before we address this additional contribution, let us discuss the values obtained for the parameters. If we know the isoenergetic jump rate  $\nu_0 \exp(-2\gamma r)$ , we can derive the lifetime  $\tau_0$  of the geminate e-h pair from the  $\tau_0\nu_0 \exp(-2\gamma r)$  value.

As an estimate, we consider first the jump rate of an electron from an optically excited donor to a silicon nanoparticle as an acceptor in a P3HT/Si solar cell, which was recently reported.<sup>9</sup> Using ultrafast pump-probe spectroscopy, Herrmann and coworkers showed that the exciton state, created instantaneously during the rise of the laser pulse, decays to yield a polaron signal. The time constant of the exciton decay and the concomitant polaron rise was found to be 120 fs, corresponding to a jump rate of  $8 \cdot 10^{12} \text{ s}^{-1}$ . This jump rate associated with the initial charge transfer step can be taken as the rate for an isoenergetic jump. Second, one may argue that the rate for an isoenergetic jump should be of the same range of that of a charge carrier in an ordered organic solid. There, the charge carrier mobility is around  $1 \text{ cm}^2/\text{Vs}$ .<sup>48</sup> By using the Einstein ratio between mobility  $\mu$  and the carrier diffusion constant  $D$ ,  $\mu/D = e/kT$ , and assuming isotropic diffusion in a cubic system, where  $D = \frac{1}{6}a^2[\nu_0 \exp(-2\gamma r)]$ , with a typical lattice constant for a crystal of 0.6 nm, one ends up with an estimate of the jump rate of  $4 \cdot 10^{13} \text{ s}^{-1}$ . Adopting a representative value for  $\tau_0\nu_0 \exp(-2\gamma r) \cong 3800$  and a jump rate of about  $4 \cdot 10^{13} \text{ s}^{-1}$  thus yields a lifetime of about 95 ps for the geminate e-h pair, which is a realistic lifetime.

The relative effective masses obtained from the simulation decrease in line with the increase in conjugation length of the compounds. This confirms the notion that improved electronic coupling along the polymer chain is crucial for improving the dissociation efficiency. However, the values for the relative effective masses  $m_{\text{eff}}/m_e$  range from 0.3 for DOOPPP to 0.060 for PCDTBT, which is rather low. For comparison, for polydiacetylene, which is the most ordered conjugated polymer that is known, electroreflectance measurements by Weiser and Möller yielded an effective mass of  $0.05 m_e$ ,<sup>49</sup> and theoretical calculations by Van der Horst placed its effective mass at  $0.1 m_e$ .<sup>50</sup> In the more disordered compounds studied here, the effective mass can be expected to be somewhat higher. Thus, in summary, while the incorporation of the conjugation lengths' effects through the effective mass leads to an improved description of the charge dissociation process, in particular for

the well-delocalized compounds, the values required for the effective mass to account for the dissociation are too low.

The fact that there must be an additional factor that contributes to efficient exciton dissociation at the D-A interface had already been noticed by Arkhipov a decade ago.<sup>23</sup> This was prompted by the observation that in a D-A system, the dissociation yield increases abruptly above a critical acceptor concentration.<sup>51</sup> Dissociation yields exceeding 50% at moderate electric field strengths, as well as the usually weak temperature and field dependence, were taken as an indication that the Coulomb attraction between carriers within a short geminate pair must be effectively screened or counterbalanced. To allow for such a screening, Arkhipov *et al.* invoke the existence of a layer of dipoles that exist in the dark (i.e., in the ground state) at the interface between donors and acceptors with different electron affinities. There are experimental and theoretical results in favor of this notion.<sup>18–20</sup> Arkhipov thus extended the effective mass model to account for the effect of dipoles.<sup>23</sup> We refer to the resulting model as the dipole model.

Arkhipov considered a bilayer system where photoexcitation results in a hole on the first chain adjacent to the interface and an electron on the acceptor on the other side of the interface [Fig. 5(b)]. Suppose there is an additional partial positive charge on the donor chain 1 and a partial negative one on the acceptors, caused by interfacial dipoles. The hole executes zero-point oscillations, as described previously, for the effective mass model, but now these oscillations occur within the Coulomb potential modified by the fractional positive charges, thus raising the energy of the hole on chain 1. A jump of the hole to chain 2 is favorable for two reasons. First, the attractive Coulomb force to the negative sibling charge is partially shielded due to the positive fractional charges on chain 1. Second, on chain 2, the energy of the zero-point oscillations is diminished since the Coulomb potential there is wider and shallower (as there are no fractional charges on chain 2). Both effects will reduce the energy needed to overcome the attractive Coulomb potential. Note that this mechanism requires internal interfaces that can exist in a bilayer system or in a blend system where phase separation occurs. In the model by Arkhipov, the interfacial dipoles are, however, not formed in a donor phase doped by a low concentration of acceptors.

Meanwhile, Wiemer *et al.*<sup>25</sup> improved the theoretical treatment and showed that the existence of a dipole layer has a profound effect. For the practical implementation, we follow the formulation by Wiemer, though for simplicity, we used a square grid with the distance between the chains equal to the distance between the dipoles equal to  $r$ . As before, the dissociation yield  $\varphi(F)$  is given by (3) and (4). The hole energy  $E_n$  is given by the sum of its kinetic energy and potential energy,

$$E_n = E_{p,n} + E_{k,n}, \quad \text{where} \quad E_{p,n} = U(x_n, y)|_{y=0} \quad \text{and} \\ E_{k,n} = \frac{1}{2}\hbar\omega = \frac{\hbar}{2\sqrt{m_{\text{eff}}}} \sqrt{\frac{d^2}{dy^2} U(x_n, y)|_{y=0}}, \quad (6)$$

which uses a parabolic approximation for the energy of the zero-point oscillations. The potential energy is modified compared to (5) by considering the effect of dipoles with

fractional strength  $\alpha$ .

$$U(y, x_n) = \frac{e^2}{4\pi\epsilon_0\epsilon_r} \frac{-1}{\sqrt{x_n^2 + y^2}} \\ + \frac{e^2}{4\pi\epsilon_0\epsilon_r} \left( \sum_{j=-N/2}^{N/2} \frac{\alpha}{\sqrt{(x_n - r)^2 + (y - (j + \frac{1}{2})r)^2}} \right. \\ \left. + \sum_{i=-N/2}^{N/2} \frac{-\alpha}{\sqrt{x_n^2 + (y - (i + \frac{1}{2})r)^2}} \right) - eFx_n. \quad (7)$$

The number  $N$  of dipoles we used is 200. For  $r$  we took 0.92 nm as before, and values for the dipole fraction  $\alpha$  were derived from the work function difference  $\Delta\Phi$  obtained from the photoemission experiments (Table I). The change in work function  $\Delta\Phi$  can be related to the fractional dipole strength  $\alpha$  at the interface using the Helmholtz equation for interfacial dipoles. When  $\Delta\Phi$  is measured in eV, the strength of an interfacial dipole can be expressed as  $\epsilon_0\epsilon_r \frac{\Delta\Phi}{e} = e\rho\sigma$ , where  $p = \alpha er$  is the dipole moment and  $\sigma$  is the area density of dipoles,  $\sigma = 1/r^2$ , with  $\sigma$  being the fractional dipole. This yields  $\alpha = \epsilon_0\epsilon_r r \Delta\Phi / e$ . Using the measured values for  $\Delta\Phi$  and taking  $\epsilon_r = 3.5$  and  $r = 0.92$  nm, we arrive at the rather low values for  $\alpha$  up to 0.03 listed in Table I. Inserting (7) into (6) allows us to simulate the dissociation yield  $\varphi(F)$  using (3) and (4) as before. The resulting curves shown in Fig. 4(c) are very similar to those of the pure effective mass model in two respects, noting, however, that the values for the effective masses are larger (vide infra). First, we can reproduce the field dependence and, in particular, the decrease of  $F_{\text{sat}}$  in the polymer series, from DOOPPP to PCDTBT. Second, the comparison of experimental and theoretical efficiencies still indicates that at lower electric fields the model predicts lower yields than experimentally measured.

To compare the simulation parameters of the dipole model with the effective mass model, we need to take a little detour. In the effective mass model, we could use accurate values for  $E_n$  by solving the Schrödinger Equation (5) numerically. This is valuable and needed when evaluating the resulting simulation parameters quantitatively. In the dipole model (6), a numerical solution to  $E_n$  was not possible, and the quantization energy needs to be approximated by a harmonic oscillator [ $U(y)$  in Fig. 5(a)]. Since we want to directly compare how the incorporation of dipoles affects the simulation and its associated parameters, we have first repeated the simulations to the effective mass model using also the harmonic oscillator approximation (Eq. 12 in Ref. 24), while keeping the effective masses equal to those obtained with the numerical solution [Table II, “effective mass model (parabolic approximation)”. The resulting field dependence of the photocurrent yield is identical to Fig. 4(b) and is therefore not shown. Changes caused by the parabolic approximation are manifested in the different values obtained for the factor  $\tau_0\nu_0 \exp(-2\gamma r)$ , which reduces by one to two orders of magnitude and shall not be considered any further. Having used the same level of approximation and very similar values for  $\tau_0\nu_0 \exp(-2\gamma r)$ , we can now consider the impact of including the dipoles on the effective masses (Table II, dipole model). We find  $m_{\text{eff}}/m_e$  still decreases from DOOPPP to MeLPPP, yet the values are

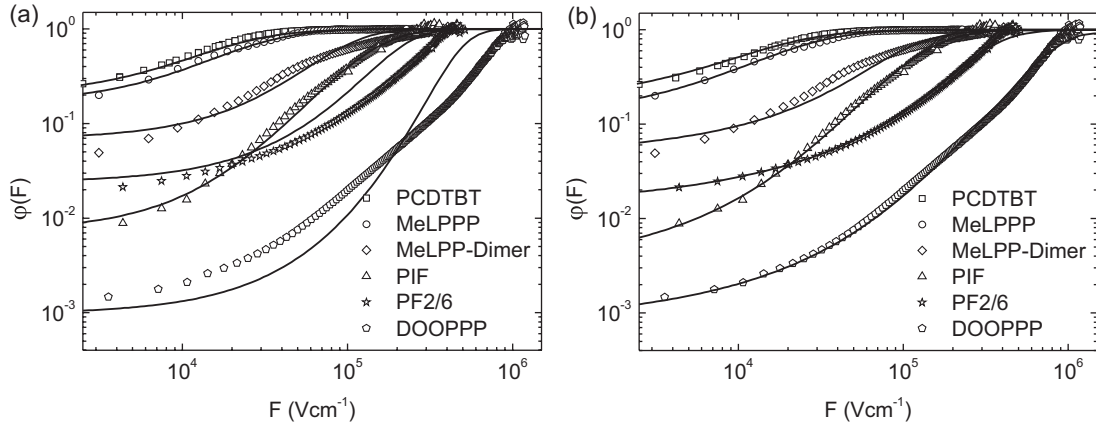


FIG. 6. Comparison of the field-dependent photocurrent yields (symbols) of donor / $C_{60}$  bilayer solar cells with simulations (lines) based on (a) the combination of dipole model with Braun model, and (b) the combination of dipole model with dopant assisted dissociation model. The parameters are presented in Table III.

higher and more realistic than those needed when the dipoles are ignored. Thus, we have seen that charge dissociation in the more efficient, well-delocalized polymers PCDTBT, MeLPPP, and PIF can be described well by taking into account the effects from both, zero-point oscillations and interfacial dipoles. For the efficient polymers with shorter conjugation length, PF2/6 and DOOPPP, there is an additional photocurrent at lower fields that is not yet included in the modeling.

### B. Combined models

We now attend to the additional contribution to the dissociation yield observed experimentally at lower electric fields. It is tempting to consider localized charge transfer states as candidates for the additional contribution. To test this hypothesis we tried to fit that extra contribution employing the Onsager-Braun model, i.e., we combined the dipole model and the Onsager-Braun model as  $\varphi(F) = \varphi_{\text{dipole}}(F) + (1 - \varphi_{\text{dipole}}(F))\varphi_{\text{Onsager-Braun}}(F)$ . As is evident in Fig. 6(a) and Table III, this was unsuccessful. To reproduce the yield at low electric fields, one had to invoke parameters that lead to a lower saturation field than experimentally observed, and, vice versa, if the saturation field is reproduced, the yields at low field cannot be matched. We therefore abandoned the Braun model (and its modification by Tachiya) to describe our results.

As a second option, we explored the idea of *dopant-assisted carrier photogeneration* at  $C_{60}$  molecules that may have diffused into the polymer donor layer.<sup>52</sup> The field dependence of the photocurrent resulting from such a process has been worked out by Arkhipov in 2003 as a variation of the effective mass model.<sup>22</sup> Arkhipov *et al.* consider a polymer film containing a low dopant concentration. The idea is again that the electron is transferred to the dopant, leaving behind a hole that oscillates coherently in the conjugated polymer segment. Due to the isolated, localized nature of the dopant, no interfacial dipoles are considered, which is in contrast to the situation of an extended dopant layer forming an interface. Note that while the dopant concentration is low and dopants are isolated within the polymer matrix, the concentration needs to be sufficient to allow for trap-to-trap motion of the

electrons to the electrode in order for this process to result in a photocurrent.

If an exciton initially happens to be on a conjugated polymer segment adjacent to an individual  $C_{60}$  molecule at a distance  $r$ , then the probability  $w$  for it to dissociate into free carriers is given by the product of the probability for the electron to transfer to the  $C_{60}$ ,  $w_t$ , multiplied by the probability for the hole to escape from the mutual Coulomb potential,  $w_{\text{esc}}$ . For an exciton with lifetime  $\tau_0$  and a tunneling rate to  $C_{60}$  given by  $k_t = \nu_0 \exp(-2\gamma r)$ , this yields

$$w_t = \frac{k_t}{k_t + \tau_0^{-1}} = \frac{1}{1 + (\nu_0 \tau_0)^{-1} \exp(2\gamma r)}. \quad (8)$$

Similarly,  $w_{\text{esc}}$  is given by considering the escape rate  $k_{\text{esc}} = \nu_0 \exp(-(U_{\text{max}} - E_{\text{min}})/kT)$  and the recombination rate, which is equal to the tunneling rate  $k_t$ . Thus,

$$w_{\text{esc}} = \frac{k_{\text{esc}}}{k_{\text{esc}} + k_t} = \frac{1}{1 + \exp(-2\gamma r) \exp\left(\frac{U_{\text{max}} - E_{\text{min}}}{kT}\right)}. \quad (9)$$

The potential  $U$  considered here is the sum of Coulomb potential and electric field, as expressed in (5). As indicated in Fig. 5(a),  $U_{\text{max}}$  is the maximum value of the potential.  $E_{\text{min}}$  is the energy of the hole. Analogous to (6), it can be expressed as the sum of the potential energy at the hole position  $x_{\text{min}}$  and the zero-point oscillation energy, so that  $E_{\text{min}} = U(x_{\text{min}}) + 0.5\hbar\omega$ . To facilitate the calculations, the parabolic approximation is used for  $\omega$  analogous to (6). The difference between  $U_{\text{max}}$  and  $E_{\text{min}}$  is the height of the barrier that the hole needs to overcome in order to escape. The probability for dissociation at a site at distance  $r$  is then

$$w(r) = \frac{1}{1 + (\nu_0 \tau_0)^{-1} \exp(2\gamma r)} \cdot \frac{1}{1 + \exp(-2\gamma r) \exp\left(\frac{U_{\text{max}} - E_{\text{min}}}{kT}\right)}. \quad (10)$$

Arkhipov considers that the dopants are distributed randomly so that the probability of finding the nearest dopant over the distance  $r$  from a conjugated segment is determined by the Poisson distribution  $P(r) = 2\pi r l N_d \exp(-\pi l N_d (r^2 - r_{\text{min}}^2))$ .

TABLE III. Fit parameter for different combined models

Material	PCDTBT	MeLPPP	PIF	PF2/6	DOOPPP	MeLPP-dimer
Dipole model + Onsager-Braun model						
$m_{\text{eff}}/m_e$ (dipole)	0.125	0.110	0.135	0.310	1.180	0.180
$\tau_0\nu_0 \exp(-2\gamma r)$	39	40	39	38	12	40
$r_0$ [nm]	0.92	0.92	0.92	0.92	0.92	0.92
$\mu\tau$ [ $10^{-12}$ m <sup>2</sup> V <sup>-1</sup> ]	5.00	4.00	0.15	0.40	0.02	1.50
Dipole model + dopant model						
$m_{\text{eff}}/m_e$ (dipole)	0.125	0.110	0.135	0.310	1.180	0.180
$\tau_0\nu_0 \exp(-2\gamma r)$	39	40	39	38	12	40
$m_{\text{eff}}/m_e$ (dopant)	0.125	0.133	0.250	0.490	1.300	0.340
$\tau_0\nu_0$ [ $10^3$ ]	55	36	22	15	8	36
$\gamma$ [nm <sup>-1</sup> ]	2.8	3.0	4.0	4.0	7.0	6.3
$\tau_0\nu_0 \exp(-2\gamma r)^a$	318	120	14	9	0.02	0.3
$r_{\text{min}}$ [nm]	0.60	0.60	0.60	0.63	0.70	0.60
$lN_d$ [ $10^{18}$ m <sup>-2</sup> ]	1.32	1.98	4.86	1.32	3.6	1.8

<sup>a</sup>Calculated from the parameters  $\tau_0\nu_0$  and  $\gamma$ , using  $r = 0.92$  nm.

$r_{\text{min}}$  is the smallest possible distance between dopant and chain,  $l$  is the conjugation length, and  $N_d$  is the dopant concentration. The overall dissociation yield  $\varphi(F)$  is then obtained by integrating  $P(r)w(r)$  over space [Eq. (8) in Ref. 22]. By combining the dipole model with the dopant-assisted model, the experimental data can be fitted in a perfect manner, giving the parameters in Table III. The high quality of fit for all polymers considered over the entire field range is very satisfying [Fig. 6(b)].

We shall consider the values obtained for the parameters. The two physical processes that are combined here in the fashion  $\varphi(F) = \varphi_{\text{dipole}}(F) + (1 - \varphi_{\text{dipole}}(F))\varphi_{\text{dopant}}(F)$  are (i) the dissociation at an interface between an extended polymer phase and an extended C<sub>60</sub> phase, where interfacial dipoles can form, and (ii) the dissociation at localized polymer/C<sub>60</sub> sites that arise from the diffusion of individual C<sub>60</sub> molecules into the polymer phase. It is gratifying that the values for the effective mass inferred from the data for both processes are close (Table III). Those values should, indeed, be similar because both processes are based upon the concept of a hole oscillating within the conjugated segment of the polymer. They differ insofar that, at the extended interface, the oscillation happens in the Coulomb well modified by the interfacial dipoles, yet at always the same distance from the C<sub>60</sub>. In contrast, for the dopant-assisted dissociation process, the Coulomb potential is only due to the geminate charges, yet the polymer-C<sub>60</sub> distance varies, and thus the position of the hole within the potential well. At this point, it is appropriate to consider the numerical error that might arise if the built-in potential, used to calculate the internal field, was 100 meV or 200 meV lower than the open-circuit voltage  $V_{\text{oc}}^{\text{photo}}$  determined for the photocurrent. Repeating the fits for such a case (see Supplemental Material<sup>26</sup>) shows that the effective masses change by up to 30%, yet they remain within the error margin indicated in Fig. 7. In view of the large variation of effective mass between the compounds, this variation obtained when using a different built-in potential is not significant.

We now turn to the remaining parameters. To evaluate whether the values obtained for  $lN_d$  are reasonable, consider a conjugation length  $l$  of about 10 nm and take the result of

$lN_d = 2 \cdot 10^{18}$  m<sup>-2</sup> obtained for MeLPPP as representative example. This translates into a dopant concentration of  $N_d = 2 \cdot 10^{20}$  cm<sup>-3</sup>. A typical concentration of molecules in a molecular crystal is about  $4 \cdot 10^{21}$  cm<sup>-3</sup> (using, for anthracene, a density of 1.2 g/cm<sup>3</sup>, a molar mass of 178g, and Avogadro's number). Assuming a similar concentration of conjugated segments (chromophores) here, this would suggest a doping concentration of about 5%. This is a realistic value. Similarly, the value obtained for  $r_{\text{min}}$  is plausible. Considering the values for the product of the lifetime and probability in detail is not meaningful. As discussed previously, they are underestimated due to the technical need of using the parabolic approximation for the potential. Nevertheless, it is encouraging that their trend and magnitude is consistent with that obtained for the effective mass model when also using the parabolic approximation.

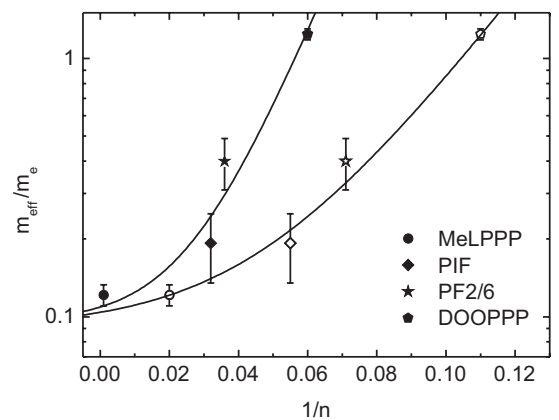


FIG. 7. The dependence of the relative effective masses on the inverse effective conjugation length of the donors for the ground state geometry (data taken from absorption, empty symbols) and for the excited state geometry (data taken from emission, filled symbols). The effective masses are taken from the dipole model (Table II) and the dipole model + dopant model (Table III), with the error bar indicating the spread of values between these models. The solid lines are fits to an exponential curve with a baseline, as described in the text.

Overall, the combination of experiment and modeling demonstrates that taking into account the effect of conjugation length by an effective mass approach is essential for an appropriate description of the dissociation process. In this context, it is useful to recall that the degree of delocalization can be quantified through the effective conjugation length. It is the number of repeat units over which an excitation, be it an exciton or a charge carrier, is coherently coupled considering, though, that there is, on average, no sharp boundary between different conjugated segments but rather a gradual local decrease of the coupling strength. In this sense, the effective mass should be viewed as an average effective mass that depends on the size of coherently coupled repeat units. The concept of a conjugation length-dependent effective mass is confirmed by Fig. 7. It shows the variation of the values for the effective mass inferred from the data fits on the reciprocal effective conjugation lengths taken from either the absorption or fluorescence spectra. The effective mass decreases roughly exponentially toward a value of about  $0.1 m_e$  at infinite conjugation length. This value is in good agreement with both experiment<sup>49</sup> and theory<sup>50</sup> on perfect  $\pi$ -conjugated chains. Empirically, the dependence of the relative effective mass on the effective conjugation lengths in either the ground state geometry (i.e., for the energy taken from the  $S_1 \leftarrow S_0$  0-0 transitions seen in absorption) or the excited state geometry (i.e., for the energy taken from the  $S_1 \rightarrow S_0$  0-0 transitions seen in fluorescence) can be expressed as

$$\frac{m_{\text{eff}}}{m_e} = 0.090 + 0.014 \cdot e^{\frac{40}{n}} \quad (11a)$$

for the excited state geometry, and

$$\frac{m_{\text{eff}}}{m_e} = 0.095 + 0.014 \cdot e^{\frac{74}{n}} \quad (11b)$$

for the ground state geometry.

This is an entirely empirical relationship, obtained for the poly(*p*-phenylene) type polymers, since for these materials the parameterization of transition energy versus conjugation lengths is known.<sup>30</sup>

#### IV. CONCLUSIONS

The present experiments on polymeric donor/ $C_{60}$  bilayer systems demonstrate that measuring the photocurrent over a broad range of electric field provides a unique source of information on the elementary step of photodissociation.

(i) The existence of a saturation field confirms the notion that mobile charge carriers originate from the dissociation of geminately bound e-h pairs. These are generated by a preceding ultrafast charge transfer step.<sup>9,10</sup>

(ii) The experiments show that the Coulomb-binding energy, evidenced by  $F_{\text{sat}}$ , scales inversely with the conjugation length of the donor polymer. If that conjugation length is large, the Coulomb-binding energy is small, and the built-in potential of the solar cell can be sufficient to break up all initially generated geminate e-h pairs. This is the case desired for solar cell applications, and it is associated with a high fill factor. Here, this is realized for MeLPPP and PCDTBT, with the latter having a far more suitable optical gap for actual solar cell applications. In contrast, if the conjugation length is short, the hole cannot overcome the Coulomb barrier and will recombine

eventually with its sibling electron. The recombination can be prevented, and escape from the Coulomb well can be assisted by supplying additional activation energy, for example, in the form of an infrared light pulse as demonstrated by Bakulin *et al.*<sup>12</sup>

(iii) Photoemission measurements and modeling show that in a bilayer device, the dissociation process can be facilitated by a weak ground state dipole layer that exists at the donor-acceptor interface and that screens the Coulomb potential.

(iv) Except for electric field strengths that are much lower than the saturation field strengths, the experimental results can be quantitatively explained in terms of a model that was set up by Arkhipov *et al.* and subsequently refined and extended by Nenashev *et al.*<sup>22-25</sup> The key idea is that the hole on the e-h pair is delocalized within a segment of the  $\pi$ -conjugated polymer and executes zero-point oscillations within the Coulomb potential well of the localized electron at the  $C_{60}$ . The energy of those zero-point oscillations is controlled by the effective mass of the hole.

(v) When modeling the experimental results, we find that the effective mass correlates inversely with the effective conjugation length, i.e., the larger the conjugation lengths, the smaller the effective mass and, concomitantly, the Coulomb-binding energy of the dissociating e-h pair.

(vi) The present results show there is also an additional photogeneration channel. It originates from the dissociation of e-h pairs at individual  $C_{60}$  molecules that diffused into the donor layer. The description of this process is also based on an effective mass model except for the absence of the interfacial dipole layer. This channel is relevant at low fields for polymers with short conjugation lengths. In systems with large effective conjugation lengths of the polymeric donor, this contribution of dopant-assisted dissociation becomes virtually negligible.

#### V. EXPERIMENTAL METHODS

MeLPPP, MeLPP-dimer, PIF, PF2/6, and DOOPPP were synthesized by the group of U. Scherf, as described elsewhere.<sup>53-56</sup> PCDTBT was bought from “1-material.” The structure formulae for the materials are given in Fig. 1. For photocurrent measurements, bilayer solar cell devices were fabricated using structured ITO-coated glass substrates in a special device architecture that eliminates edge effects.<sup>16</sup> This allows applying electric fields up to 1.3 MV/cm without risking spurious breakdown effects. For the series of solar cells reported here, 50–60-nm-high conductive PEDOT:PSS (Sigma Aldrich, neutral pH) was spin coated on top of the ITO and heated up to 180 °C for 30 min. Onto this, 40-nm-thick polymer films were spin coated from filtered chlorobenzene solutions (5.0–7.5 mg/ml) and annealed at 80 °C for 10 min to remove any residual solvent. This was followed by vapor deposition of a 40-nm layer of  $C_{60}$  (99.9% purity, AmericanDyeSourceInc). A 100-nm vapor-deposited layer of aluminum as a top electrode completed the diode structure.

Current-voltage curves were measured under monochromatic illumination at 2.2 eV (570 nm) from a 150 W Xenon lamp at 1.5 mW/cm<sup>2</sup>. At this wavelength, the light is absorbed by the  $C_{60}$  acceptor while the polymer donors are not excited, except for the low-bandgap polymer PCDTBT. The photocurrent was determined by measuring the dark current

and the total current under illumination and then subtracting the dark current from the total current under illumination. This is done after each data point before stepping to the next voltage step. The solar cells were evaporated under a vacuum of  $5 \cdot 10^{-7}$  mbar at room temperature. A Keithley 236 source-measure unit was used to record current and applied voltage. The internal electric field was calculated as  $|F| = (V - V_{bi})/d$ , where  $V$  is the applied external voltage,  $V_{bi}$  is the built-in field, taken as  $V_{bi} = V_{oc}^{photo}$  unless stated otherwise.  $V_{oc}^{photo}$  is the open-circuit voltage determined for the photocurrent (i.e., after subtracting the dark current from the total current).

Its value is slightly higher than that of the usual open-circuit voltage,  $V_{oc}$ , where the total current (dark current + photocurrent) is zero.  $d$  is the active film thickness determined using a Dektak surface profilometer. The relative photocurrent quantum yield  $\varphi(F)$  corresponds to the photocurrent per illuminated light intensity, both normalized to unit area.  $\varphi(F)$  is normalized to unity at the high field saturation value. In our earlier work,<sup>16</sup> we have confirmed that  $\varphi(F)$  indeed is on the order of unity at the high field saturation value by considering the absorption coefficient and modeling the exciton diffusion to the interface. The incident light intensities were recorded with a calibrated Hamamatsu S1337-33BQ photodiode, and the absorption of the films was measured using a Cary 5000 absorption spectrometer.

For UPS studies, the polymer samples were spincoated on PEDOT:PSS coated ITO glass substrates from chlorobenzene solutions (2 mg/ml, 25 rps), similar as previously described.

$C_{60}$  was vacuum sublimed (base pressure  $p = 3 \cdot 10^{-9}$  mbar) from resistively heated glass crucibles. The mass thickness of the layers was monitored using a quartz crystal microbalance [ $\rho(C_{60}) = 1.6 \text{ g/cm}^3$ ]. The UPS measurements were performed using a multitechnique ultra high vacuum (UHV) apparatus (base pressure:  $1 \cdot 10^{-10}$  mbar) and a Helium discharge lamp ( $h\nu = 21.22 \text{ eV}$ ). The initial photon flux was attenuated by a factor of  $\sim 100$  using a silicon filter to avoid irradiation damage of the sample. All spectra were recorded at room temperature and normal emission using a hemispherical Specs Phoibos 100 energy analyzer with 90 meV energy resolution. To determine the work function, the SECO was recorded with the sample biased at  $-10 \text{ V}$  to clear the analyzer work function. Binding energies are reported relative to the Fermi-level spectra, and the error of energy values is estimated to be  $\pm 0.05 \text{ eV}$ .

## ACKNOWLEDGMENTS

We thank the group of Prof. Ullrich Scherf for supplying the ladder type polymers and dimer and Prof. J. P. Rabe for providing access to a photoelectron spectroscopy setup. This work was supported by the GRK 1640 and the SPP1355 of the Deutsche Forschungsgemeinschaft (DFG), the Helmholtz-Energie-Allianz ‘‘Hybrid-Photovoltaik,’’ and the network ‘‘SolTechGoHybrid’’ of the Bayerische Staatsministerium f ur Wissenschaft, Forschung und Kunst.

\*Corresponding author: [anna.koehler@uni-bayreuth.de](mailto:anna.koehler@uni-bayreuth.de)

- <sup>1</sup>Heliatek, [http://www.heliatek.com/wp-content/uploads/2013/01/130116\\_PR\\_Heliatek\\_achieves\\_record\\_cell\\_efficiency\\_for\\_OPV.pdf](http://www.heliatek.com/wp-content/uploads/2013/01/130116_PR_Heliatek_achieves_record_cell_efficiency_for_OPV.pdf), 2013.
- <sup>2</sup>L. M uller-Meskamp, Y. H. Kim, T. Roch, S. Hofmann, R. Scholz, S. Eckardt, K. Leo, and A. F. Lasagni, *Adv. Mater.* **24**, 906 (2012).
- <sup>3</sup>C. M uller, T. A. M. Ferenczi, M. Campoy-Quiles, J. M. Frost, D. D. C. Bradley, P. Smith, N. Stingelin-Stutzmann, and J. Nelson, *Adv. Mater.* **20**, 3510 (2008).
- <sup>4</sup>J. Y. Kim, K. Lee, N. E. Coates, D. Moses, T. Q. Nguyen, M. Dante, and A. J. Heeger, *Science* **317**, 222 (2007).
- <sup>5</sup>C. Deibel and V. Dyakonov, *Rep. Prog. Phys.* **73**, 096401 (2010).
- <sup>6</sup>R. H. Friend, M. Phillips, A. Rao, M. W. B. Wilson, Z. Li, and C. R. McNeill, *Faraday Discuss.* **155**, 339 (2012).
- <sup>7</sup>J. L. Br edas, J. E. Norton, J. Cornil, and V. Coropceanu, *Acc. Chem. Res.* **42**, 1691 (2009).
- <sup>8</sup>J. Nelson, *Mater Today* **14**, 462 (2011).
- <sup>9</sup>D. Herrmann, S. Niesar, C. Scharsich, A. K ohler, M. Stutzmann, and E. Riedle, *J. Am. Chem. Soc.* **133**, 18220 (2011).
- <sup>10</sup>F. Etzold, I. A. Howard, R. Mauer, M. Meister, T. D. Kim, K. S. Lee, N. S. Baek, and F. Laquai, *J. Am. Chem. Soc.* **133**, 9469 (2011).
- <sup>11</sup>T. M. Clarke and J. R. Durrant, *Chem. Rev.* **110**, 6736 (2010).
- <sup>12</sup>A. A. Bakulin, A. Rao, V. G. Pavelyev, P. H. M. van Loosdrecht, M. S. Pshenichnikov, D. Niedzialek, J. Cornil, D. Beljonne, and R. H. Friend, *Science* **335**, 1340 (2012).

- <sup>13</sup>T. G. J. van der Hofstad, D. Di Nuzzo, M. van den Berg, R. A. J. Janssen, and S. C. J. Meskers, *Adv. Energy Mater.* **2**, 1095 (2012).
- <sup>14</sup>C. Deibel, T. Strobel, and V. Dyakonov, *Phys. Rev. Lett.* **103**, 036402 (2009).
- <sup>15</sup>A. K ohler, D. A. dos Santos, D. Beljonne, Z. Shuai, J. L. Br edas, A. B. Holmes, A. Kraus, K. M ullen, and R. H. Friend, *Nature* **392**, 903 (1998).
- <sup>16</sup>C. Schwarz, H. B assler, I. Bauer, J. M. Koenen, E. Preis, U. Scherf, and A. K ohler, *Adv. Mater.* **24**, 922 (2012).
- <sup>17</sup>A. J. Heeger, *Chem. Soc. Rev.* **39**, 2354 (2010).
- <sup>18</sup>S. Verlaak, D. Beljonne, D. Cheyng, C. Rolin, M. Linares, F. Castet, J. Cornil, and P. Heremans, *Adv. Funct. Mater.* **19**, 3809 (2009).
- <sup>19</sup>A. Ojala, A. Petersen, A. Fuchs, R. Lovrincic, C. P olking, J. Trollmann, J. Hwang, C. Lennartz, H. Reichelt, H. W. H offken, A. Pucci, P. Erk, T. Kirchartz, and F. W urthner, *Adv. Funct. Mater.* **22**, 86 (2012).
- <sup>20</sup>H. Aarnio, P. Sehati, S. Braun, M. Nyman, M. P. de Jong, M. Fahlman, and R.  osterbacka, *Adv. Energy Mater.* **1**, 792 (2011).
- <sup>21</sup>R. R. Chance and C. L. Braun, *J. Chem. Phys.* **59**, 2269 (1973).
- <sup>22</sup>V. I. Arkhipov, E. V. Emelianova, and H. B assler, *Chem. Phys. Lett.* **372**, 886 (2003).
- <sup>23</sup>V. I. Arkhipov, P. Heremans, and H. B assler, *Appl. Phys. Lett.* **82**, 4605 (2003).
- <sup>24</sup>A. V. Nenashev, S. D. Baranovskii, M. Wiemer, F. Jansson, R.  osterbacka, A. V. Dvurechenskii, and F. Gebhard, *Phys. Rev. B* **84**, 035210 (2011).

- <sup>25</sup>M. Wiemer, A. V. Nenashev, F. Jansson, and S. D. Baranovskii, *Appl. Phys. Lett.* **99**, 013302 (2011).
- <sup>26</sup>See Supplemental Material at <http://link.aps.org/supplemental/10.1103/PhysRevB.87.155205> for (i) an estimate of the critical photon density at which geminate and non-geminate recombination become comparable, (ii) more parameters for the Braun model, (iii) the photocurrent yield and fits to the MeLPP-Dimer, (iv) parameters and fits to the combined Dipole model + Dopant model using different values for the built-in field.
- <sup>27</sup>B. P. Rand, D. Cheyns, K. Vasseur, N. C. Giebink, S. Mothy, Y. P. Yi, V. Coropceanu, D. Beljonne, J. Cornil, J. L. Brédas, and J. Genoe, *Adv. Funct. Mater.* **22**, 2987 (2012).
- <sup>28</sup>W. Kuhn, *Helv. Chim. Acta* **31**, 1780 (1948).
- <sup>29</sup>J. Gierschner, J. Cornil, and H. J. Egelhaaf, *Adv. Mater.* **19**, 173 (2007).
- <sup>30</sup>S. T. Hoffmann, H. Bässler, and A. Köhler, *J. Phys. Chem. B* **114**, 17037 (2010).
- <sup>31</sup>K. Akaike, K. Kanai, H. Yoshida, J. Tsutsumi, T. Nishi, N. Sato, Y. Ouchi, and K. Seki, *J. Appl. Phys.* **104**, 023710 (2008).
- <sup>32</sup>J. Niederhausen, P. Amsalem, A. Wilke, R. Schlesinger, S. Winkler, A. Vollmer, J. P. Rabe, and N. Koch, *Phys. Rev. B* **86**, 081411 (2012).
- <sup>33</sup>S. Braun, W. R. Salaneck, and M. Fahlman, *Adv. Mater.* **21**, 1450 (2009).
- <sup>34</sup>H. Ishii, K. Sugiyama, E. Ito, and K. Seki, *Adv. Mater.* **11**, 605 (1999).
- <sup>35</sup>M. Körner, F. Loske, M. Einax, A. Kühnle, M. Reichling, and P. Maass, *Phys. Rev. Lett.* **107**, 016101 (2011).
- <sup>36</sup>A. C. Morteani, P. Sreearunothai, L. M. Herz, R. H. Friend, and C. Silva, *Phys. Rev. Lett.* **92**, 247402 (2004).
- <sup>37</sup>D. Veldman, Ö. Ipek, S. C. J. Meskers, J. Sweelssen, M. M. Koetse, S. C. Veenstra, J. M. Kroon, S. S. van Bavel, J. Loos, and R. A. J. Janssen, *J. Am. Chem. Soc.* **130**, 7721 (2008).
- <sup>38</sup>L. Onsager, *Phys. Rev.* **54**, 554 (1938).
- <sup>39</sup>C. L. Braun, *J. Chem. Phys.* **80**, 4157 (1984).
- <sup>40</sup>K. K. H. Chan, S. W. Tsang, H. K. H. Lee, F. So, and S. K. So, *Org. Electron.* **13**, 850 (2012).
- <sup>41</sup>R. A. Marsh, J. M. Hodgkiss, and R. H. Friend, *Adv. Mater.* **22**, 3672 (2010).
- <sup>42</sup>C. S. Ponceca, A. Yartsev, E. Wang, M. R. Andersson, D. Vithanage, and V. Sundström, *J. Am. Chem. Soc.* **134**, 11836 (2012).
- <sup>43</sup>J. Kirkpatrick, P. E. Keivanidis, A. Bruno, F. Ma, S. A. Haque, A. Yarstev, V. Sundström, and J. Nelson, *J. Phys. Chem. B* **115**, 15174 (2011).
- <sup>44</sup>M. Wojcik and M. Tachiya, *J. Chem. Phys.* **130**, 104107 (2009).
- <sup>45</sup>S. Barth, H. Bässler, U. Scherf, and K. Müllen, *Chem. Phys. Lett.* **288**, 147 (1998).
- <sup>46</sup>A. Petersen, A. Ojala, T. Kirchartz, T. A. Wagner, F. Würthner, and U. Rau, *Phys. Rev. B* **85**, 245208 (2012).
- <sup>47</sup>N. Christ, S. W. Kettlitz, S. Valouch, J. Mescher, M. Nintz, and U. Lemmer, *Org. Electron.* **14**, 973 (2013).
- <sup>48</sup>M. Pope and C. E. Swenberg, *Electronic Processes in Organic Crystals and Polymers* (Oxford University Press, New York, 1999).
- <sup>49</sup>G. Weiser and S. Möller, *Phys. Rev. B* **65**, 045203 (2002).
- <sup>50</sup>J. W. van der Horst, P. A. Bobbert, M. A. J. Michels, and H. Bässler, *J. Chem. Phys.* **114**, 6950 (2001).
- <sup>51</sup>C. Im, W. Tian, H. Bässler, A. Fechtenkötter, M. D. Watson, and K. Müllen, *J. Chem. Phys.* **119**, 3952 (2003).
- <sup>52</sup>D. E. Markov, E. Amsterdam, P. W. M. Blom, A. B. Sieval, and J. C. Hummelen, *J. Phys. Chem. A* **109**, 5266 (2005).
- <sup>53</sup>M. Grell, W. Knoll, D. Lupo, A. Meisel, T. Miteva, D. Neher, H. G. Nothofer, U. Scherf, and A. Yasuda, *Adv. Mater.* **11**, 671 (1999).
- <sup>54</sup>S. P. Huang, G. S. Huang, and S. A. Chen, *Synth. Met.* **157**, 863 (2007).
- <sup>55</sup>U. Scherf and K. Müllen, *Makromol Chem-Rapid* **12**, 489 (1991).
- <sup>56</sup>S. Setayesh, D. Marsitzky, and K. Müllen, *Macromolecules* **33**, 2016 (2000).